The role of the resonance modes in the response of a fluid-loaded structure

Paul J.T. Filippi, Dominique Habault, Pierre-Olivier Mattei, Cédric Maury

The role of the resonance modes in the response of a fluid-loaded structure

P. J. T. FILIPPI
Ecole Supérieure de Mécanique de Marseille, Technopole de Château-Gombert,
13451 Marseille cedex 20, France

D. HABAULT AND P.-O. MATTEI
C.N.R.S. Laboratoire de Mécanique et d'Acoustique, 31 chemin Joseph Aiguier,
13402 Marseille cedex 20, France

C. MAURY
Institute of Sound and Vibration Research, The University, Southampton S017 1BJ, England

This paper is concerned with problems of fluid/structure interaction. The aim is to show how the resonance modes can be used to describe the response of a fluid-loaded structure (displacement of the structure and sound pressure in the fluid) for any kind of excitation (periodic, randomly dependent on time and space, or transient). First, the expression of the response of the system in terms of resonance modes is recalled. To compute the resonance modes, it is necessary to solve a system of equations in the harmonic regime. Several numerical methods are considered and a comparison of their respective efficiency is presented. Finally, two examples of applications are studied in detail. Namely, a thin plate excited by a turbulent wall pressure and a thin shell excited by a transient acoustic signal. For this last example, some experimental data are compared with numerical results.

1. INTRODUCTION

The number of publications on fluid/structure interactions over the past three decades is quite impressive. Let us only mention some of the most important books recently published on this topic. The earliest one is due to Junger and Feit [1], the first edition of which appeared in 1972. Then two books were published in the 1980s [2, 3]. These three books provide a very complete overview of the knowledge in the domain and the physics of the phenomena is presented in a classical way which is very easy to follow. A more recent text book [4] proposes a very rigorous mathematical statement of the problem together with the most recent numerical methods. Let us also mention the CISM Course [5] in which the basic concepts of the fluid/structure interaction phenomena are described. Finally, a very interesting analytical study is due to Crighton [6] who points out the efficiency of asymptotic techniques.

This paper shows how the resonance modes can be used to describe the response of a fluid-loaded structure (displacement of the structure and sound pressure in the fluid). Most of the results concerning the interaction between a vibrating structure and a fluid, mainly those involving a heavy fluid, show that the response of the structure is governed by

the fluid-loaded resonance modes. Their role seems essential for large bandwidth excitations (as, for example, turbulent wall pressure) or transient excitations. It is then interesting to develop numerical methods based on the expansion of the response of the system into a series of the fluid-loaded resonance modes.

This paper summarizes some results previously obtained by the authors [7–12]. It also includes three original parts.

The first one is a presentation of the theoretical development which is more general than the ones given previously (see reference [5], for example). The second one is a comparison of the efficiency of several numerical methods used to solve the equations of the boundary value problem. The comparison is made on a one-dimensional example. The third one deals with the diffraction of a transient acoustic wave by an axially symmetrical shell (*Line*-2′ shape): numerical predictions are compared with experimental results.

Section 2 is devoted to the description of the equations. The excitation can be harmonically time dependent, transient or random in space and time. First, the response of the system to a harmonic excitation is expanded into a series of eigenmodes which depend on frequency. By using a Fourier inverse transform, it is then possible to express the response of the system to a transient excitation in terms of the fluid-loaded structure resonance modes. These modes do not depend on frequency. When the resonance modes are known, the response of the system to any kind of excitation is obtained. The coefficients of the series are given in an explicit form, which, in general, cannot be computed numerically. Nevertheless, these coefficients can also be obtained as solutions of an infinite system of linear equations which can be solved approximately by a truncation procedure.

Section 3 presents several numerical methods for solving the equations corresponding to the harmonic regime and a comparison of their efficiency on a simple example. The example chosen is a one-dimensional baffled plate, in contact with a heavy fluid (water) on one side, and with a *vacuum* on the other side; the plate is clamped at its boundaries. Two groups of methods are described.

In the first group, the equations are transformed into boundary integral equations by using the Green representations for the displacement and the sound pressure. The system obtained is solved by three numerical kinds of approximations. The unknown functions are successively approximated by piecewise constant functions, then by truncated series of orthogonal polynomials (Legendre or Tchebycheff). A third method consists of approximating the displacement by polynomial functions which satisfy the boundary conditions for the plate displacement, and the acoustic pressure by polynomials. In the second group, the Green representation of the acoustic pressure is still used but the plate equation is written in a variational form. The pressure is approximated by a truncated series of Legendre polynomials, while the plate displacement is approximated by Legendre polynomial functions which satisfy the boundary equations. The pressure/displacement relationship is replaced by a system of "adapted" collocation equations; the plate equation is replaced by the corresponding Ritz–Galerkin equations.

Section 4 presents the first example: a rectangular baffled plate excited by a wall pressure induced by a turbulent flow. The model of turbulent wall pressure is the one proposed by Corcos [13]. The power density spectrum of the plate displacement is computed by solving a sequence of harmonic equations. For a given frequency, the problem is transformed into a system of Boundary Integral Equations and the unknown functions are approximated by truncated series of Tchebycheff polynomials. The coefficients are solutions of the "adapted" collocation equations. The power density spectrum of the plate displacement shows sharp peaks for each resonance frequency of the fluid-loaded structure.

Section 5 presents the second example: a *Line* 2′ shell excited by a transient incident sound wave. The response of the system is expressed as a truncated series of the fluid-loaded

structure resonance modes. These modes are calculated by using the variational formulation and polynomial functions satisfying the boundary conditions. The sound pressure diffracted by the shell is calculated and compared to experimental results: the agreement is quite good.

2. GENERAL STATEMENT OF THE PROBLEM

Consider a thin shell occupying a surface Σ and denote by Ω the exterior domain; Σ is assumed to have everywhere a unit external normal vector $\mathbf{n}$. The shell is made of an elastic material characterized by a density μ, a Young modulus E and the Poisson ratio ν; its thickness is denoted by h. It is immersed in a fluid which extends to infinity and which is characterized by a density μ_0 and a sound speed c_0; its interior is a *vacuum* (see Figure 1). For simplicity, it is assumed that all the mechanical and geometrical characteristics of the system are constant. In this section, the superscript " $\sim$ " is used for functions which depend on time. The capital letters $\mathbf{F}$, $\mathbf{U}$ and $\mathbf{P}$ denote vector functions.

The system is excited by a force density $\tilde{\mathbf{F}}$ applied to the shell and an incident acoustic pressure $\tilde{p}_i$, both of which are zero outside a time interval $[0, T]$, $\tilde{\mathbf{F}}$ is square integrable in time and space, while $\tilde{p}_i$ is square integrable in time and on any space domain of finite dimension (this corresponds to a finite energy excitation).

Let $\tilde{\mathbf{U}}$ be the displacement vector of the shell with components $(\tilde{u}_1, \tilde{u}_2, \tilde{u}_3)$: the first two ones are tangent to Σ, the third one is normal and positive when pointing out to the exterior of the shell. The sound field radiated by the shell is denoted by $\tilde{p}_S$. The equations governing the response of the system have the following form:

$$\mathbf{A}\tilde{\mathbf{U}} + \mu h\ddot{\tilde{\mathbf{U}}} + \tilde{\mathbf{P}}_S = \tilde{\mathbf{F}} - \tilde{\mathbf{P}}_i \quad \text{on } \Sigma,$$

$$\Delta\tilde{p}_S - (1/c_0^2)\ddot{\tilde{p}}_S = 0 \quad \text{in } \Omega,$$

$$\mu_0\ddot{\tilde{u}}_3 + \operatorname{Tr}\partial_n\tilde{p}_S = -\operatorname{Tr}\partial_n\tilde{p}_i \quad \text{on } \Sigma. \tag{1}$$

Here the matrix $\mathbf{A}$ is the partial derivative operator which describes the shell properties. The notation $\operatorname{Tr} f$ stands for the limit value of the function f when the current point in Ω tends to

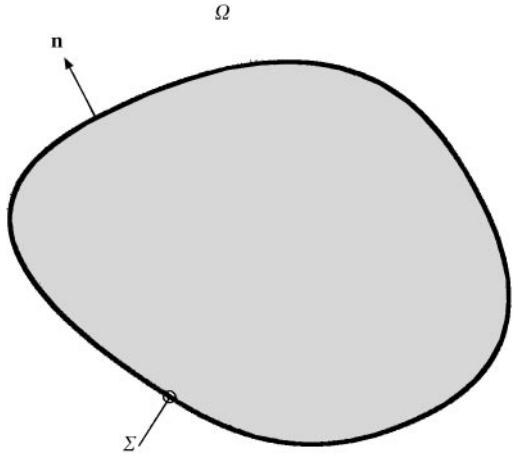

Figure 1. Sketch of the fluid-loaded structure.

a point on Σ: this notation is necessary when f has a discontinuity across Σ or is expressed by an integral which becomes hyper-singular on Σ (this occurs with layer potentials). $\tilde{\mathbf{P}}_S$ is the vector $(0, 0, \mathrm{Tr}\,\tilde{p}_S)$ and $\tilde{\mathbf{P}}_i$ is the vector $(0, 0, \mathrm{Tr}\,\tilde{p}_i)$. The notation $\ddot{f}$ stands for the second partial derivative of f with respect to time. These equations are completed by initial conditions (for example, every function and its first time derivative is zero for $t < 0$), by boundary conditions and, if needed, by continuity conditions on $\tilde{\mathbf{U}}$. An outgoing wave condition is also added for $\tilde{p}_S$.

In the domain Ω, the acoustic pressure field $\tilde{p}_S$ can be represented by a boundary integral in terms of a layer density $\tilde{\bar{\omega}}$, that is,

$$\tilde{p}_S = \tilde{\mathscr{K}}\,\tilde{\bar{\omega}}, \tag{2}$$

where $\tilde{\mathscr{K}}$ is an integral operator. In general, its kernel will be any linear combination of the freefield Green kernel of the wave equation and its normal derivative (see its Fourier transform in equation (8)). For simple geometries (baffled plate, for example), use can be made of the Green function which satisfies the Neumann boundary condition on Σ.

The values of $\tilde{p}_S$ and of its normal derivative on the shell surface Σ can be written as

$$\mathrm{Tr}\,\tilde{p}_S = \tilde{\mathscr{K}}_1\,\tilde{\bar{\omega}}, \quad \mathrm{Tr}\,\partial_n \tilde{p}_S = \tilde{\mathscr{K}}_2\,\tilde{\bar{\omega}}, \tag{3}$$

where $\tilde{\mathscr{K}}_1$ and $\tilde{\mathscr{K}}_2$ are related to $\tilde{\mathscr{K}}$ in a very simple way.

The system of equations (1) is then replaced by

$$\begin{aligned} &\mathbf{A}\tilde{\mathbf{U}} + \mu h\ddot{\tilde{\mathbf{U}}} + \tilde{\tilde{\mathscr{K}}}_1\,\tilde{\bar{\omega}} = \tilde{\mathbf{F}} - \tilde{\mathbf{P}}_i \quad \text{on } \Sigma, \\ &\mu_0 \ddot{\tilde{u}}_3 + \tilde{\mathscr{K}}_2\,\tilde{\bar{\omega}} = -\,\mathrm{Tr}\,\partial_n \tilde{p}_i \quad \text{on } \Sigma. \end{aligned} \tag{4}$$

Let us note that the first equation is a vector equation where $\tilde{\tilde{\mathscr{K}}}_1\,\tilde{\bar{\omega}}$ is the vector $(0, 0, \tilde{\mathscr{K}}_1\,\tilde{\bar{\omega}})$. The second equation is scalar. All the unknown functions are defined on the shell surface only. These equations can also be written in a variational form (which corresponds to the energy balance)

$$\begin{aligned} &\mathscr{A}(\tilde{\mathbf{U}}, \tilde{\mathbf{V}}) + \int \mathrm{d}t \int_\Sigma \mu h[\ddot{\tilde{\mathbf{U}}} + \tilde{\tilde{\mathscr{K}}}_1\,\tilde{\bar{\omega}}] \cdot \tilde{\mathbf{V}}^* \,\mathrm{d}\Sigma = \int \mathrm{d}t \int_\Sigma [\tilde{\mathbf{F}} - \tilde{\mathbf{P}}_i] \cdot \tilde{\mathbf{V}}^* \,\mathrm{d}\Sigma, \\ &\int \mathrm{d}t \int_\Sigma [\mu_0 \ddot{\tilde{u}}_3 + \tilde{\mathscr{K}}_2\,\tilde{\bar{\omega}}]\,\tilde{\Psi}^* \,\mathrm{d}\Sigma = -\int \mathrm{d}t \int_\Sigma \mathrm{Tr}\,\partial_n \tilde{p}_i\,\tilde{\Psi}^* \,\mathrm{d}\Sigma, \end{aligned} \tag{5}$$

where $\tilde{\mathbf{V}}$ and $\tilde{\Psi}$ are test functions, $\mathscr{A}(\tilde{\mathbf{U}}, \tilde{\mathbf{V}})$ is the bilinear form corresponding to the expression of the potential energy of the shell, $(\,)^*$ denotes a complex conjugate and $\mathbf{U} \cdot \mathbf{V}$ is the scalar product of the two vectors $\mathbf{U}$ and $\mathbf{V}$. In the following, all integration elements will be omitted unless there is any ambiguity.

2.1. HARMONIC REGIME AND EIGENMODES SERIES

The basic idea developed in this subsection and in the next one is the same as that used by Morse and Ingard [14] (section 9.5 on Room Acoustics) for the evaluation of the acoustic response of a room to either a harmonic or a transient source. They consider a room with absorbing walls and make several assumptions. Though the physical system is not conservative, for any excitation frequency the existence of eigenmodes and eigenvalues which are frequency dependent is assumed; the response of the room to any source is expanded into a series of these eigenmodes. The response of the room to a transient

excitation is then determined by an inverse Fourier transform which is calculated by the residues method under the following hypotheses: the eigenmodes and eigenfrequencies depend analytically on the frequency; the coefficients of the harmonic response expansion have poles only (no branch cuts) which correspond to the resonance frequencies (free oscillations) of the room. We do not know any general mathematical justification of this theoretical approach. But as long as an analytical solution exists (separation of variables), this approach can be applied. From a physicist's point of view, what is true for a parallelepipedic enclosure should remain true for any other shape of practical interest.

For the present problem, the vibro-acoustic response of a fluid-loaded shell, it can be proved that the forthcoming developments are valid in very simple situations. We, thus, assume that they remain valid for any situation. We will precise the assumptions made at each step.

Let f be the time Fourier transform of a function $\tilde{f}$ defined as it is usual in acoustics by

$$f(\omega) = \int_{-\infty}^{+\infty} \tilde{f}(t) \mathrm{e}^{\mathrm{i}\omega t} \, \mathrm{d}t. \tag{6}$$

Equations (5) become

$$\mathscr{A}(\mathbf{U}, \mathbf{V}) + \int_{\Sigma} [- \omega^2 \mu h \mathbf{U} + \bar{\mathscr{K}}_1^{\omega} \bar{\omega}] \cdot \mathbf{V}^* = \int_{\Sigma} [\mathbf{F} - \mathbf{P}_i] \cdot \mathbf{V}^*,$$

$$\int_{\Sigma} [- \omega^2 \mu_0 u_3 + \mathscr{K}_2^{\omega} \bar{\omega}] \Psi^* = - \int_{\Sigma} \mathrm{Tr}\, \partial_n p_i \Psi^*, \tag{7}$$

where $\bar{\mathscr{K}}_1^{\omega}$ and $\mathscr{K}_2^{\omega}$ are the Fourier transforms of the operators $\tilde{\bar{\mathscr{K}}}_1$ and $\tilde{\mathscr{K}}_2$. They depend on the angular frequency ω. More precisely, the integral representation of the acoustic pressure field, its value and the value of its normal derivative on Σ can be written as

$$p_S(M) = \mathscr{K}^{\omega} \bar{\omega} = \int_{\Sigma} [G(M, M') + \kappa \partial_{n(M')} G(M, M')] \bar{\omega}(M') \, \mathrm{d}M',$$

$$\begin{aligned} \mathrm{Tr}\, p_S(M) &= \mathscr{K}_1^{\omega} \bar{\omega} \\ &= - \frac{\kappa \bar{\omega}(M)}{2} + \int_{\Sigma} [G(M, M') + \kappa \partial_{n(M')} G(M, M')] \bar{\omega}(M') \, \mathrm{d}M', \\ \mathrm{Tr}\, \partial_n p_S(M) &= \mathscr{K}_2^{\omega} \bar{\omega} \\ &= - \frac{\bar{\omega}(M)}{2} + Pf \int_{\Sigma} \partial_{n(M)} [G(M, M') + \kappa \partial_{n(M')} G(M, M')] \bar{\omega}(M') \, \mathrm{d}M', \end{aligned} \tag{8}$$

where $G(M, M') = - \exp(\mathrm{i}\omega r(M, M')/c_0)/(4\pi r(M, M'))$ is the freefield Green kernel of the Helmholtz equation which satisfies the Sommerfeld condition corresponding to the time dependence, κ is a function of ω with non-zero imaginary part and such that $\kappa(-\omega^*) = \kappa^*(\omega)$, and the symbol Pf denotes the finite part of the hyper-singular integral. With this choice, the operator $\mathscr{K}_2^{\omega}$ has an inverse $\{\mathscr{K}_2^{\omega}\}^{-1}$ for any real frequency, that is the function $\bar{\omega}$ can be calculated for any given ω and $\mathrm{Tr}\, p_S$.

Finally, replacing the unknown function $\bar{\omega}$ by χ:

$$\chi = \bar{\omega}/\omega^2 \mu_0, \tag{9}$$

one gets

$$\mathscr{A}(\mathbf{U},\mathbf{V}) - \omega^2\mu h \int_\Sigma \left[\mathbf{U} - \frac{\mu_0}{\mu h}\,\bar{\mathscr{K}}_1^\omega \chi\right]\cdot \mathbf{V}^* = \int_\Sigma [\mathbf{F} - \mathbf{P}_i]\cdot \mathbf{V}^*,$$

$$\int_\Sigma [-u_3 + \mathscr{K}_2^\omega \chi]\,\Psi^* = -\frac{1}{\omega^2\mu_0}\int_\Sigma \operatorname{Tr}\partial_n p_i \Psi^*. \tag{10}$$

Let us define the eigenmodes and eigenvalues of equation (10). Their existence, which can be proved in very simple situations, is assumed for the general case. Introducing the notation $\hat{\mathbf{U}}_n = (\hat{u}_{n1}, \hat{u}_{n2}, \hat{u}_{n3})$, the eigenmodes $(\hat{\mathbf{U}}_n, \hat{\chi}_n)$ and eigenvalues Λ_n satisfy the following system of homogeneous equations:

$$\mathscr{A}(\hat{\mathbf{U}}_n,\mathbf{V}) - \Lambda_n \int_\Sigma \left[\hat{\mathbf{U}}_n - \frac{\mu_0}{\mu h}\,\bar{\mathscr{K}}_1^\omega \hat{\chi}_n\right]\cdot \mathbf{V}^* = 0, \quad \int_\Sigma [-\hat{u}_{n3} + \mathscr{K}_2^\omega \hat{\chi}_n]\Psi^* = 0. \tag{11}$$

From the last equation, $\hat{\chi}_n$ can be expressed as a function of $\hat{u}_{n3}$:

$$\hat{\chi}_n = \mathscr{Y}_2^\omega \hat{u}_{n3}, \tag{12}$$

where $\mathscr{Y}_2^\omega$ is the symbolic inverse of $\mathscr{K}_2^\omega$.

The system of equations (11) reduce to one equation only

$$\mathscr{A}(\hat{\mathbf{U}}_n,\mathbf{V}) - \Lambda_n \int_\Sigma \left[\hat{\mathbf{U}}_n - \frac{\mu_0}{\mu h}\bar{\mathscr{K}}_1^\omega(\mathscr{Y}_2^\omega \hat{u}_{n3})\right]\cdot \mathbf{V}^* = 0. \tag{13}$$

The eigenmodes and eigenvalues depend on the angular frequency. It can be shown [15] that the eigenmodes satisfy the following orthogonality relationship:

$$\begin{aligned}\mathscr{A}(\hat{\mathbf{U}}_n \hat{\mathbf{U}}_m^*) &= \Lambda_n \int_\Sigma \left[\hat{\mathbf{U}}_n - \frac{\mu_0}{\mu h}\bar{\mathscr{K}}_1^\omega \hat{\chi}_n\right]\cdot \hat{\mathbf{U}}_m = 0 \qquad \text{if } m \neq n \\ &= N_n^2(\omega) \qquad\qquad\qquad\qquad\qquad\qquad\qquad\qquad \text{if } m = n.\end{aligned} \tag{14}$$

Here, N_n can be seen as playing a role equivalent to the norm of $\hat{\mathbf{U}}_n$.

The displacement $\mathbf{U}$, solution of equations (10) is sought as a series of the eigenmodes:

$$\mathbf{U} = \sum_n \alpha_n \hat{\mathbf{U}}_n. \tag{15}$$

By introducing this series and using the formal inverse of $\mathscr{K}_2^\omega$, the system of equations (10) is replaced by the following equation:

$$\sum_n \alpha_n \left\{\mathscr{A}(\hat{\mathbf{U}}_n,\mathbf{V}) - \omega^2\mu h \int_\Sigma \left[\hat{\mathbf{U}}_n - \frac{\mu_0}{\mu h}\,\bar{\mathscr{K}}_1^\omega(\mathscr{Y}_2^\omega \hat{u}_{n3})\right]\cdot \mathbf{V}^*\right\}$$

$$= \int_\Sigma [\mathbf{F} - \mathbf{P}_i + \bar{\mathscr{K}}_1^\omega(\mathscr{Y}_2^\omega \operatorname{Tr}\partial_n p_i]\cdot \mathbf{V}^*. \tag{16}$$

To determine the coefficients of the expansion of $\mathbf{U}$, this equation is written for $\mathbf{V} = \mathbf{U}_m^*$. An explicit form of the operator $\mathscr{Y}_2^\omega$ is not needed. Indeed, the Green formula applied to the functions

$$\Phi_i = \mathscr{K}^\omega(\mathscr{Y}_2^\omega \operatorname{Tr} \partial_n p_i) \quad \text{and} \quad \hat{\psi}_m = \mathscr{K}^\omega \hat{\chi}_n \tag{17}$$

leads to the following equality:

$$\int_\Sigma \mathscr{K}^\omega(\mathscr{Y}_2^\omega \operatorname{Tr} \partial_n p_i)\hat{u}_{m3} = \int_\Sigma \operatorname{Tr} \partial_n p_i \operatorname{Tr} \hat{\psi}_m. \tag{18}$$

This result together with the orthogonality relationship provides the following expression for the coefficients α_n:

$$\alpha_n = -\frac{\Lambda_n}{N_n^2(\omega)(\omega^2 \mu h - \Lambda_n)} \int_\Sigma [(\mathbf{F} - \mathbf{P}_i)\cdot \hat{\mathbf{U}}_n + \operatorname{Tr} \partial_n p_i \operatorname{Tr} \hat{\psi}_n]. \tag{19}$$

Finally, the acoustic pressure radiated by the shell is given by the series

$$p_S = \sum_n \alpha_n \hat{p}_n + p_N \tag{20}$$

with

$$\hat{p}_n = \mu_0 \omega^2 \mathscr{K}^\omega \hat{\chi}_n \quad \text{and} \quad p_N = -\mathscr{K}^\omega(\mathscr{Y}_2^\omega \operatorname{Tr} \partial_n p_i).$$

The sum $p_i + p_N$ satisfies a homogeneous Neumann condition on the shell surface, that is p_N is the pressure field reflected by a perfectly rigid structure. The result is summarized as follows:

$$\mathbf{U} = \sum_{n=1}^{\infty} \alpha_n \hat{\mathbf{U}}_n, \quad p_S = \mu_0 \omega^2 \sum_{n=1}^{\infty} \alpha_n \hat{\psi}_n + p_N,$$

$$\alpha_n = -\frac{\Lambda_n \Phi_n}{N_n^2(\omega)(\omega^2 \mu h - \Lambda_n)}, \quad \Phi_n = \int_\Sigma [(\mathbf{F} - \mathbf{P}_i)\cdot \hat{\mathbf{U}}_n + \operatorname{Tr} \partial_n p_i \operatorname{Tr} \hat{\psi}_n], \tag{21}$$

where all the quantities involved, considered as functions of the complex variable ω satisfy the following relationship:

$$f(-\omega^*) = f^*(\omega) \tag{22}$$

for any real excitation (transient force and incident acoustic pressure).

2.2. TRANSIENT REGIME AND RESONANCE MODES

The transient response of the system is obtained by taking the inverse Fourier transform of the harmonic displacement and pressure field. This leads to a representation of the solution in terms of the resonance modes of the fluid-loaded structure (free oscillation modes).

The existence of the resonance modes and of the resonance frequencies has been proved for three-dimensional elasticity [16]. It is assumed that the results of this reference are still valid for the thin-body approximate equations of elasticity.

The resonance modes $(\mathbf{U}_n, p_n)$ of the structure/fluid system and the resonance angular frequencies ω_n are defined by

$$\mathscr{A}(\mathbf{U}_n, \mathbf{V}) - \omega_n^2 \mu h \int_\Sigma \left[\mathbf{U}_n - \frac{\mu_0}{\mu h} \mathscr{K}_1^{\omega_n} \chi_n \right] \cdot \mathbf{V}^* = 0,$$

$$\int_\Sigma [- u_{n3} + \mathscr{K}_2^{\omega_n} \chi_n] \Psi^* = 0, \quad p_n = \mu_0 \omega_n^2 \mathscr{K}^{\omega_n} \chi_n. \tag{23}$$

The resonance frequencies ω_n are related to the eigenvalues Λ_n defined in the previous paragraph by

$$\omega_n^2 \mu h = \Lambda_n(\omega_n). \tag{24}$$

It has been shown that, for any $n \neq 0$, this equation has two solutions that we denote ω_n and ω_{-n}. They have the following property [16]:

$$\omega_n = \Omega_n - \mathrm{i}\tau_n \quad \text{with } \Omega_n > 0,\ \tau_n > 0, \quad \omega_{-n} = -\omega_n^*. \tag{25}$$

The inverse Fourier transforms to be calculated have the following form:

$$\tilde{F}(t) = \frac{1}{2\pi} \int_{-\infty}^{+\infty} \frac{f(\omega)}{N_n^2(\omega)(\omega^2 \mu h - \Lambda_n)} \mathrm{e}^{-\mathrm{i}\omega t} \, \mathrm{d}\omega. \tag{26}$$

The use of the method of residues immediately leads to

$$\tilde{F}(t) = -\mathrm{i}\mathrm{Y}(t) \left[\frac{f(\omega_n)}{N_n^2(\omega_n)[2\omega_n \mu h - \Lambda_n'(\omega_n)]} \mathrm{e}^{-\mathrm{i}\omega_n t} - \frac{f^*(\omega_n)}{N_n^{*2}(\omega_n)[2\omega_n^* \mu h - \Lambda_n'^*(\omega_n)]} \mathrm{e}^{\mathrm{i}\omega_n^* t} \right], \tag{27}$$

where $\mathrm{Y}(t)$ is the Heaviside step function and $\Lambda_n'(\omega)$ is the derivative of Λ_n with respect to ω; use has been made of the result $\Lambda_n'(-\omega^*) = -\Lambda_n^{*\prime}(\omega)$ which is deduced from the property of $\Lambda_n(\omega)$ given in equation (22). The function $\tilde{F}(t)$ is real valued. Thus, the transient response of the system has the expression:

$$\tilde{\mathbf{U}}(t) = \mathrm{i}\mathrm{Y}(t) \sum_{n=1}^{\infty} \left[\frac{\Lambda_n(\omega_n) \Phi_n(\omega_n)}{N_n^2(\omega_n)[2\omega_n \mu h - \Lambda_n'(\omega_n)]} \mathbf{U}_n \mathrm{e}^{-\mathrm{i}\Omega_n t} \right.$$

$$\left. - \frac{\Lambda_n^*(\omega_n) \Phi_n^*(\omega_n)}{N_n^{*2}(\omega_n)[2\omega_n^* \mu h - \Lambda_n'^*(\omega_n)]} \mathbf{U}_n^* \mathrm{e}^{\mathrm{i}\Omega_n t} \right] \mathrm{e}^{-\tau_n t},$$

$$\tilde{p}(t) = \tilde{p}_i(t) + \tilde{p}_N(t) + \mathrm{i}\mathrm{Y}(t) \sum_{n=1}^{\infty} \left[\frac{\Lambda_n(\omega_n) \Phi_n(\omega_n)}{N_n^2(\omega_n)[2\omega_n \mu h - \Lambda_n'(\omega_n)]} p_n \mathrm{e}^{-\mathrm{i}\Omega_n t} \right.$$

$$\left. - \frac{\Lambda_n^*(\omega_n) \Phi_n^*(\omega_n)}{N_n^{*2}(\omega_n)[2\omega_n^* \mu h - \Lambda_n'^*(\omega_n)]} p_n^* \mathrm{e}^{\mathrm{i}\Omega_n t} \right] \mathrm{e}^{-\tau_n t}, \tag{28}$$

where Y is the Heaviside function. This kind of expression is used in example 2 (section 5).

This result is based on the following hypotheses. The eigenmodes and the eigenvalues depend analytically on the frequency (this is reasonable because they are solutions of an

equation which depends analytically on the frequency). As a consequence, the factors $N_n(\omega)$ have the same property; furthermore, it is assumed that they have no zero.

Let us make a final comment on the expansions in resonance modes.

By applying the time Fourier transform to expression (28), one gets a representation of the response of the system to a harmonic excitation in terms of resonance modes:

$$\mathbf{U}(\omega) = \mathrm{i} \sum_{n=1}^{\infty} \left[\frac{\Lambda_n(\omega_n)\Phi_n(\omega_n)}{N_n^2(\omega_n)[2\omega_n\mu h - \Lambda_n'(\omega_n)]} \frac{1}{\mathrm{i}(\Omega_n - \omega) + \tau_n} \mathbf{U}_n \right.$$

$$\left. + \frac{\Lambda_n^*(\omega_n)\Phi_n^*(\omega_n)}{N_n^{*2}(\omega_n)[2\omega_n^*\mu h - \Lambda_n'^*(\omega_n)]} \frac{1}{\mathrm{i}(\Omega_n + \omega) - \tau_n} \mathbf{U}_n^* \right],$$

$$p(\omega) = p_i(\omega) + p_N(\omega) + \mathrm{i} \sum_{n=1}^{\infty} \left[\frac{\Lambda_n(\omega_n)\Phi_n(\omega_n)}{N_n^2(\omega_n)[2\omega_n\mu h - \Lambda_n'(\omega_n)]} \frac{1}{\mathrm{i}(\Omega_n - \omega) + \tau_n} p_n \right.$$

$$\left. + \frac{\Lambda_n^*(\omega_n)\Phi_n^*(\omega_n)}{N_n^{*2}(\omega_n)[2\omega_n^*\mu h - \Lambda_n'^*(\omega_n)]} \frac{1}{\mathrm{i}(\Omega_n + \omega) - \tau_n} \mathbf{U}_n^* \right]. \tag{29}$$

This last expression shows clearly that the response of the system is maximum when the excitation frequency is equal to the real part of any resonance frequency. Such a property is not pointed out by the eigenmodes series representation of the solution.

2.3. REMARKS

(1) From a purely theoretical point of view, the series representations (28) and (29) are very attractive because explicit expressions of the coefficients are given. But, in practice, they cannot be calculated easily mainly because they involve the derivative of the eigenvalues with respect to the angular frequency.

When the fluid is a gas, its influence on the vibrations of the structure is small and a perturbation method can be used to derive an approximation of the resonance modes and frequencies of the fluid-loaded structure from its *in vacuo* modes and frequencies. An approximation of expressions (28) and (29) can then be obtained. In general, the coefficients of the expansions are computed by solving a truncated form of an infinite system of algebraic linear equations.

(2) The main difficulty is to calculate the fluid-loaded resonance modes. There exists a few cases for which a method of separation of variables is available. In general, only numerical approximations can be obtained. It is then necessary to have an efficient computer program for solving the system of equations (23) which correspond to the steady state equations for any complex angular frequency.

For this reason, in the next section several numerical methods to solve equations (23) are examined for the simple example of a one-dimensional baffled plate excited by a point harmonic source. The convergence of these methods has already been proved in theoretical papers (see references [17, 18], for example). Here our point is to develop numerical comparisons. The results obtained are discussed in order to provide criteria for determining the values of the parameters corresponding to each method.

(3) Finally, it must be mentioned that the representation of the solution in terms of resonance modes is much more interesting for transient regimes. For harmonic or random excitations, a direct numerical method (finite elements, boundary elements, etc.) is often

much less time consuming. But for transient excitations, the series of resonance modes seems to be the best way to describe the successive wavefronts which are experimentally observed. For example, in reference [16], the contributions of the resonance modes are easily interpreted as surface waves.

3. COMPARISONS BETWEEN SOME NUMERICAL METHODS

The example chosen in this section is a one-dimensional baffled plate excited by a harmonic source. Two main methods are described. In the "fully integral" method, the acoustic pressure and the plate displacement are represented by integrals based on the use of the Helmholtz and plate Green kernels. In the "mixed integro-differential" method, the acoustic pressure is represented by a boundary integral, while the plate displacement is considered as the solution of a differential equation.

3.1. STATEMENT OF THE EXAMPLE

Consider a one-dimensional plate which occupies the segment $\Sigma = (-L/2 < x < +L/2)$ of the $y = 0$ axis and which is clamped at both ends. The remaining part $\Sigma' = (|x| > +L/2)$ is a perfectly rigid baffle. The half-space $\mathscr{D} = (y > 0)$ is occupied by a fluid, while the other half-space is a *vacuum*. The characteristics of the plate are: thickness h, density μ, Young's modulus E, the Poisson ratio v. The characteristics of the fluid are: density μ_0, sound speed c_0. The plate is excited by a harmonic unit point force located at $x = S$; the excitation angular frequency is ω; and there is no acoustic source.

Let w and p be the plate displacement and the acoustic pressure respectively. They satisfy the following system of equations:

$$D(\partial^4 w/\partial x^4) - \mu h\omega^2 w + P = \delta_S \quad \text{on } \Sigma,$$

$$\Delta p + k^2 p = 0 \quad \text{in } \mathscr{D},$$

$$\text{Tr } (\partial p/\partial y) = \begin{cases} \omega^2 \mu_0 w & \text{on } \Sigma \\ 0 & \text{on } \Sigma' \end{cases}$$

$$w(-L/2) = w(L/2) = w'(-L/2) = w'(L/2) = 0,$$

$$\text{with} \quad D = Eh^3/12(1 - v^2), \quad k^2 = \omega^2/c_0^2, \quad P = \text{Tr } p. \tag{30}$$

The uniqueness of the solution is ensured by adding a Sommerfeld condition on p. Let $\mathscr{G}$ be the Green function of the Helmholtz equation which satisfies a Neumann condition on $\Sigma \cup \Sigma'$ and the Sommerfeld condition. The acoustic pressure is expressed in terms of the plate displacement by

$$p = \omega^2 \mu_0 \int_\Sigma \mathscr{G} w. \tag{31}$$

Using this expression, the system of equations (30), is replaced by a system of integro-differential equations on Σ:

$$D(\partial^4 w/\partial x^4) - \mu h\omega^2 w + P = \delta_S \quad \text{on } \Sigma,$$

$$\mu_0\omega^2 \int_\Sigma \mathscr{G}w - P = 0 \quad \text{on } \Sigma,$$

$$w(-L/2) = w(L/2) = w'(-L/2) = w'(L/2) = 0. \tag{32}$$

The variational form of these equations is given by

$$\int_\Sigma \left[D\,\frac{\partial^2 w}{\partial x^2}\,\frac{\partial^2 v^*}{\partial x^2} - \mu h\omega^2 w v^* + P v^* \right] = v^*(S) \quad \text{on } \Sigma,$$

$$\int_\Sigma \left[\mu_0\omega^2 \int_\Sigma \mathscr{G}w - P \right] \Psi^* = 0 \quad \text{on } \Sigma, \tag{33}$$

where v and Ψ are test functions (see, for example, reference [4]).

Let Γ be the Green kernel of the plate equation which satisfies the Sommerfeld condition corresponding to outgoing waves. A Green's formula applied to Γ and w gives a representation of w in terms of the excitation force, the acoustic pressure and boundary sources. The system of equations (32) is thus replaced by the following system of integral equations:

$$w + \Gamma * P + \Gamma * [u_1^+ \delta_{L/2} - u_1^- \delta_{-L/2} + u_2^+ \delta'_{L/2} - u_2^- \delta'_{-L/2}] = \Gamma * \delta_S \quad \text{on } \Sigma,$$

$$\mu_0\omega^2 \int_\Sigma \mathscr{G}w - P = 0 \quad \text{on } \Sigma, \tag{34}$$

$$w(-L/2) = w(L/2) = w'(-L/2) = w'(L/2) = 0,$$

where $\Gamma * f$ stands for the convolution product of the plate Green kernel by the function f and $\delta'_a = \partial\delta_a/\partial x$ is the derivative with respect to x of the Dirac measure located in $x = a$; the scalars $u_1^\pm$ are the values of the third derivative of w at $x = \pm L/2$; the scalars $u_2^\pm$ are the values of the second derivative of w at $x = \pm L/2$. The boundary conditions provide the four additional integral equations required to determine the two unknown functions and the four boundary sources.

In the next subsections, two families of numerical methods are studied. The first family solves equations (34): two families of approximation functions are used and the system is solved by a *collocation* method. We call it the *boundary integral/collocation method*. The second family solves equations (33). The unknown functions are approximated by polynomial functions. The differential equation is approximated either by Ritz–Galerkin equations or by collocation equations, while the integral equation is approximated by collocation equations. We call it the *mixed differential-boundary integral/Ritz-collocation method*. These methods are quite classical. The aim of this section is to compare their efficiency and provide some practical rules of convergence for the particular case of a heavy fluid (water).

3.2. THE BOUNDARY INTEGRAL/COLLOCATION METHOD

The simplest approximation of the solution of equation (34) is provided by piecewise constant functions. A more refined approximation is obtained by using orthogonal polynomials.

3.2.1. *Approximation by piecewise constant functions*

The interval Σ is divided into sub-intervals σ_i centered at the points x_i. It must be remarked that the plate displacement and the acoustic pressure have not the same wavelength. Thus, two sets of sub-intervals are defined: $\sigma_i^d (i = 1, \ldots, Nd)$ for the displacement and $\sigma_i^p (i = 1, \ldots, Np)$ for the pressure. The first equation (34) is written at the centers of each interval σ_i^d, while the second one is written at the centers of each interval σ_i^p. This finally provides $(Nd + Np + 4)$ equations when the four boundary conditions are added.

The functions w and P are approximated by piecewise constant functions with values w_i and P_i on σ_i.

The accuracy of the approximations depends on two main parameters. The first one is, of course, Nd and Np which must be large enough so that the space variations of the unknown functions are correctly described. The second parameter is the accuracy of the numerical integration of the kernels Γ and $\mathscr{G}$ over each sub-interval σ_i.

3.2.2. *Approximation by orthogonal polynomials and adapted collocation*

The unknown functions are approximated by truncated series of orthogonal polynomials U_i (we have tested Legendre and Tchebycheff polynomials):

$$w \approx \sum_{i=0}^{Nd} w_i U_i, \quad P \approx \sum_{i=0}^{Np} \psi_i U_i.$$

The first equation of equation (34) is written at the zeros of the polynomial U_{Nd+1} and the second one at the zeros of the polynomial U_{Np+1}. This leads to a system of equations that are called here "adapted collocation equations". The interest of choosing these collocation points is that the equations obtained are equivalent to Ritz–Galerkin equations which are known for giving a much more accurate result (see, for example, references [7] or [15]).

It is also possible to choose for the U_i a combination of orthogonal polynomials which satisfy the boundary conditions. Thus, the four equations which express the boundary conditions and require a rather significant computing time, are no more necessary. This results in a significant computing time economy.

3.3. THE MIXED DIFFERENTIAL-BOUNDARY INTEGRAL/RITZ COLLOCATION METHOD

In this section, the acoustic pressure in equations (33) is approximated by a sum of normalized Legendre polynomials $\psi_i(x) = A_i P_i(2x/L)$ (A_i is the norm of P_i):

$$P \approx \sum_{i=0}^{Np} \bar{\omega}_i \psi_i. \tag{35}$$

The displacement is approximated by a sum of polynomial functions. These polynomial functions are linear combinations of Legendre polynomials chosen such to satisfy the boundary conditions. The displacement approximation and the approximation functions

are defined by

$$w \approx \sum_{i=0}^{Nd} w_i W_i,$$

$$W_i(x) = B_i \left[P_i\left(\frac{2x}{L}\right) - \frac{4i+10}{2i+7} P_{i+2}\left(\frac{2x}{L}\right) + \frac{2i+3}{2i+7} P_{i+4}\left(\frac{2x}{L}\right) \right], \tag{36}$$

where B_i is a normalizing factor. The function W_i is a polynomial of degree $(i+4)$. It seems reasonable to adopt the same degree of polynomial approximations for both the pressure and the displacement: thus $Np = (Nd + 4)$.

These approximations are introduced into equations (33). The test functions are chosen equal to the approximation functions, that is the equations are written for

$$v = W_i, \quad i = 1, 2, \ldots, Nd, \quad \Psi = \psi_i, \quad i = 1, 2, \ldots, Np. \tag{37}$$

The first equation (33) is replaced by the corresponding Ritz–Galerkin equations, while the second equation is replaced by the set of adapted collocation equations:

$$\sum_{i=0}^{Nd} w_i \int_\Sigma \left[D \frac{\partial^2 W_i}{\partial x^2} \frac{\partial^2 W_j}{\partial x^2} - \mu h \omega^2 W_i W_j \right] + \sum_{k=0}^{Np} \bar{\omega}_k \int_\Sigma \psi_k W_j = W_j(S), \quad j = 1, 2, \ldots, Nd,$$

$$\mu_0 \omega^2 \sum_{i=0}^{Nd} w_i \int_\Sigma \mathcal{G} W_i(X_r) - \sum_{k=0}^{Np} \bar{\omega}_k \psi_k(X_r) = 0, \quad r = 1, 2, \ldots, Np, \tag{38}$$

where the X_r are the zeros of the function ψ_{Np+1}.

The main advantage of this formulation is that the parameters D and μh can be functions of the variable x. In the first equation (38) the numerical evaluation of the integrals requires a rather large amount of time.

For constant plate parameters, the integrals involved in the left side of the first equations can be computed exactly by using a Gauss–Legendre procedure. In this case and if the excitation force is a square integrable function $F(x)$, an adapted collocation can be used and the system is replaced by

$$\sum_{i=0}^{Nd} w_i \left[D \frac{\partial^4 W_i}{\partial x^4}(Y_q) - \mu h \omega^2 W_i(Y_q) + \sum_{k=0}^{Np} \bar{\omega}_k \psi_k(Y_q) = F(Y_q), \quad q = 1, 2, \ldots, Nd, \right.$$

$$\mu_0 \omega^2 \sum_{i=0}^{Nd} w_i \int_\Sigma \mathcal{G} W_i(X_r) - \sum_{k=0}^{Np} \bar{\omega}_k \psi_k(X_r) = 0, \quad r = 1, 2, \ldots, Np, \tag{39}$$

where the Y_q are the zeros of the polynomial ψ_{Nd+1}. This approximation can be improved by using more collocation points in both of the two equations and solving the rectangular system thus obtained by a least-squares method.

In the last section, the transient vibro-acoustics response of a *Line*-2′ is studied. Though this shell has a constant thickness and is made of a homogeneous material, the elasticity equations have variable coefficients. Thus, the approximation equations which have been adopted are similar to those described in this subsection.

3.4. NUMERICAL COMPARISON BETWEEN THE TWO FAMILIES OF APPROXIMATIONS

The example studied in this section is a one-dimensional baffled plate, immersed in water and excited by a harmonic point force. The response of the system is computed by the

TABLE 1

Characteristics of the three plates

Material	E (Pa)	μ (kg m^{-3})	v	h (mm)	$\mu h/D$ (kg m^{-3} N^{-1})	CF (m^{-1})
Plate 1: steel	$2{\cdot}26 \times 10^{11}$	7800	0·28	10	$3{\cdot}82 \times 10^{-3}$	12·8
Plate 2: aluminum	$0{\cdot}73 \times 10^{11}$	2650	0·33	10	$3{\cdot}88 \times 10^{-3}$	37·7
Plate 3: aluminum	$0{\cdot}73 \times 10^{11}$	2650	0·33	3	$34{\cdot}38 \times 10^{-3}$	125·8

methods presented in the previous section. For numerical comparisons, three plates are examined. Their characteristics are summarized in Table 1. The "coupling factor" (CF) is defined as the ratio $\mu_0/\mu h$. The length of each plate is $L = 1$ m. The fluid (water) is characterized by $\mu_0 = 1000$ kg/m^3 and $c_0 = 1500$ m/s.

These three examples present a particular interest from a numerical point of view. The ratio $\mu h/D$ in the first two plates have very close values but the coupling factor is different. This means that plates 1 and 2 have very close values for their *in vacuo* eigenfrequencies but they have different resonance frequencies in water (see below). Plates 2 and 3 correspond to the same material but different thicknesses. Then, comparisons between plates 1 and 2 point out the influence of the coupling factor and comparisons between plates 2 and 3 point out the influence of the thickness of the plate. The first eigenfrequencies of the plates (*in vacuo*) and the first resonance frequencies in water are:

Eigenfrequencies:

Plate 1: 57·6, 158·9, 311·4, 514·8 Hz,
Plate 2: 57·1, 157·6, 308·8, 510·5 Hz,
Plate 3: 17·1, 47·3, 92·6, 153·2, 228·8, 319·6, 425·4, 546·5 Hz.

Resonance frequencies in water:

Plate 1: 16, 84, 188, 346 Hz,
Plate 2: 54, 125, 239, 393 Hz,
Plate 3: 9, 22, 43, 71, 109, 157, 215, 283, 362 Hz.

The two families of methods described in the previous section have been applied. Method I is the boundary integral/collocation method. The approximation functions are piecewise constant functions. Nd and Np are the numbers of constants used to approximate the displacement and the sound pressure respectively. The two series of collocation points are equally spaced on the plate. As seen before, this leads to a linear system of order $(Nd + Np + 4)$. In method I′, the collocation functions are orthogonal (Legendre or Tchebycheff) polynomials and the two series of collocation points are the zeros of the polynomials $Nd + 1$ and $Np + 1$ respectively.

Method II is the mixed differential-boundary integral/Ritz-collocation method. The displacement is approximated by polynomial functions and the sound pressure by Legendre polynomials. Nd and Np are the numbers of functions used to approximate the displacement and the sound pressure respectively. We have chosen to approximate the displacement and the pressure by polynomial functions of the same maximum degree. This corresponds to $Np = (Nd + 4)$. As mentioned above (section 3.3), if the plate excitation is a square integrable function, the Ritz equations can be replaced by a set of adapted collocation equations (method II′).

The frequencies studied range from 56 to 1500 Hz. For each frequency, the convergence has been studied by varying the values of (Nd, Np). Three types of curves have been computed: the displacement on the plate, the sound pressure on a line parallel and very close to the plate (distance $= L/40$), and the sound pressure radiated at a distance $R = 1$ m from the plate.

The convergence of each method is evaluated from comparisons on the displacement curves (on a linear-scale) only. This corresponds to the most strict conditions. In most cases, the convergence on the other two curves (sound pressure at $L/40$ and at $R = 1$ m) is reached for lower values of (Nd, Np). Let us mention that the values given in Tables 2 and 3 are not exactly the lowest values which give an accurate displacement. For each plate and frequency, 10–12 couples (Nd, Np) have been tested. The values given in the tables correspond to the lowest values tested which gave the right curve (computed with large values of (Nd, Np)) with a discrepancy less than 1%.

The results obtained with method I are summarized in Table 2. For each plate and each frequency, Table 2 gives the values (Nd, Np) and the number M of zeros of the displacement curve. In the convergence tests, the values of Np have been chosen smaller or at most equal to Nd since the most classical criterion for collocation methods applied to integral equations is simply related to the wavelength in the propagation medium. It says that the number of collocation points must be such that the length of the sub-elements is equal or less than one-sixth of the wavelength. In the examples chosen, the wavelength in the fluid is much smaller than the wavelength in the plate. For example, at 500 Hz, the wavelength in water is equal to 3 m, the wavelength in plate 1 and 2 is 0·45 m, the wavelength in plate 3 is 0·25 m.

Table 2 shows that this criterion does not apply so simply. First, the best results have been obtained for equal values of Nd and Np. Furthermore, the numbers Nd and Np clearly depend not only on the wavelength but also on the coupling factor.

Although the wavelength is the same in plates 1 and 2, Nd is larger for plate 2 for which the coupling factor is approximately three times larger than the coupling factor for plate 1. To emphasize the role of the coupling factor, let us mention the results obtained in air. For

TABLE 2

Method I—values of $(Nd - Np)$ *and* M

F (Hz)	56	120	250	250	1500
Plate 1	6–6; 1	10–10; 1	12–12; 3	30–30; 3	60–60; 7
Plate 2	30–30; 1	30–30; 2	40–40; 3	40–40; 5	80–80; 8
Plate 3	30–30; 3	40–40; 5	40–40; 8	60–60; 11	98–98; 18

TABLE 3

Method II—values of $(Nd - Np)$ *and* M

F (Hz)	56	120	250	500	1500
Plate 1	4–8; 1	7–11; 1	8–12; 3	13–17; 3	19–23; 7
Plate 2	4–8; 1	7–11; 2	9–13; 3	15–19; 5	19–23; 8
Plate 3	11–15; 3	15–19; 5	19–23; 8	26–30; 11	—

the same calculation for plate 3, only 10–01 is needed at 56 Hz and 12–07 at 120 Hz, the coupling factor is equal to $0{\cdot}16\ \mathrm{m}^{-1}$ in this case.

The same curves have been obtained with method I′, with similar values of (Nd, Np). It does not seem that using orthogonal polynomials provides any improvement, from a numerical point of view. On the contrary, for equal values of (Nd, Np), this requires a larger computing time since it includes the computation of integrals of products of polynomials and Hankel functions.

Figures 2 and 3 show two examples of convergence for the displacement on plate 2, for two frequencies 56 and 1500 Hz.

The results obtained with method II are summarized in Table 3. For each frequency and each plate, Table 3 gives the values Nd and $Np = (Nd + 4)$. M has of course the same values as in Table 2.

It can be seen that the values of Nd mainly depend on the number of maxima of the displacement. In most cases, $2M \leqslant Nd \leqslant 4\,M$. For both plates 1 and 2, values of the ratio $\mu h/D$ are very close to each other; thus, at each frequency, the value of Nd can be chosen of the same order of magnitude for both plates. It is larger for plate 3 for which the wavenumbers and then M are larger. For plate 3, we do not give any result at 1500 Hz: it

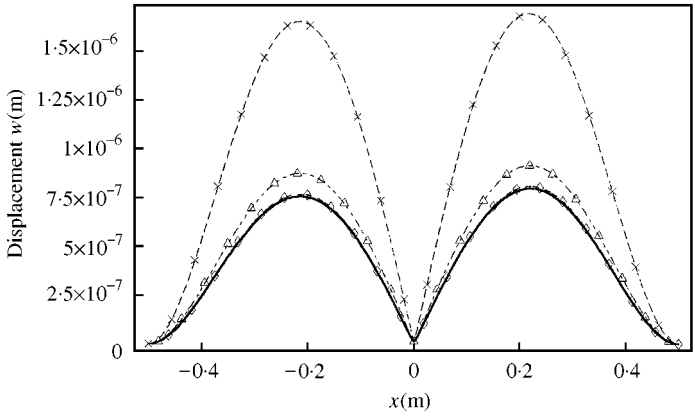

Figure 2. Plate displacement showing convergence of Method I. Plate 2 at 56 Hz (×, $Nd = 12$, $Np = 6$; △, $Nd = 18$, $Np = 20$; ◇, $Nd = 30$, $Np = 30$; continuous line $Nd = 40$, $Np = 40$).

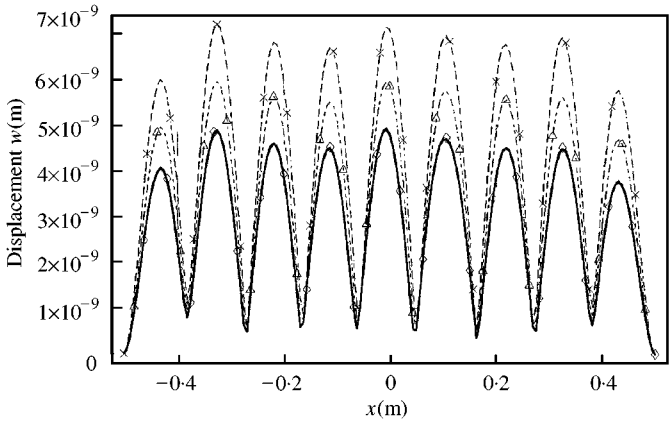

Figure 3. Plate displacement showing convergence of Method I. Plate 2 at 1500 Hz. (×, $Nd = 30$; $Np = 30$, △, $Nd = 40$, $Np = 40$; ◇, $Nd = 90$, $Np = 90$; continuous line $Nd = 98$, $Np = 98$).

appeared that the system of equations becomes unstable unless the working precision is increased (for example with a Mathematica program, the regular precision of 16 digits is not sufficient): nevertheless, by taking precautions, it has been possible to suppress these instabilities and obtain reliable results.

Figures 4 and 5 show the convergence of the method for plate 2 at 56 and 1500 Hz. Figures 6 and 7 present a comparison between the curves obtained for plate 2 with methods I and II at 56 and 1500 Hz respectively. The two methods do not give exactly the same result. The differences on the maxima is about 2% at 56 Hz, and 5% at 1500 Hz: this is absolutely not significant, the difference induced on the pressure field being much less than 0·1 dB. Nevertheless, it is necessary to give an explanation of this discrepancy. It is of course possible to prove that both approximation methods converge to the exact solution. But, in practice, due to rounding errors, the numerical results do not converge to the exact solution; furthermore, the rounding errors depending on the numerical method, a perfect agreement between various numerical approximations cannot be expected.

On a few examples, method II′ has also been tested. It appears that, for the same choice of (Nd, Np), the results have the same accuracy, but the computation time is reduced.

Finally, Figures 8 and 9 present the directivity patterns of the plates at 56 and 1500 Hz, calculated with method II.

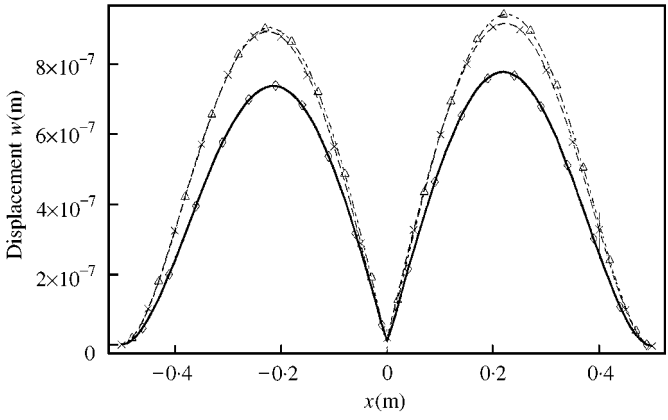

Figure 4. Plate displacement showing convergence of Method II. Plate 2 at 56 Hz. (×, $Nd = 2$; △, $Nd = 3$; ◇, $Nd = 4$; continuous line, $Nd = 5$).

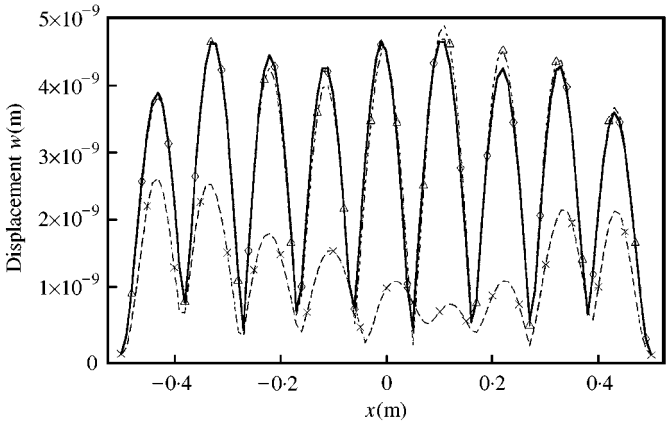

Figure 5. Plate displacement showing convergence of Method II. Plate 2 at 1500 Hz. (×, $Nd = 11$; △, $Nd = 15$; ◇, $Nd = 19$; continuous line, $Nd = 27$).

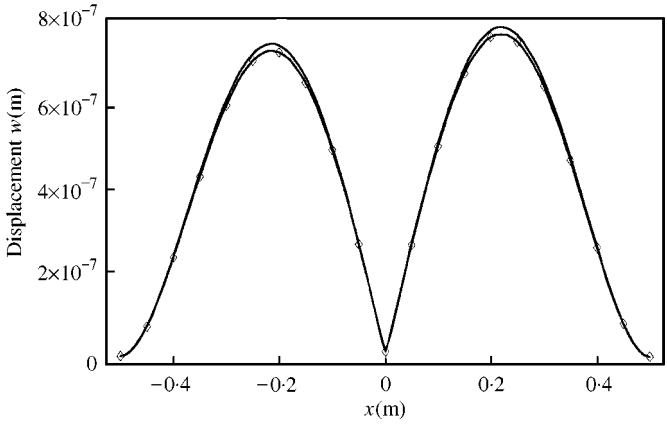

Figure 6. Comparison between methods I and II (marked with ◇) for plate 2 at 56 Hz.

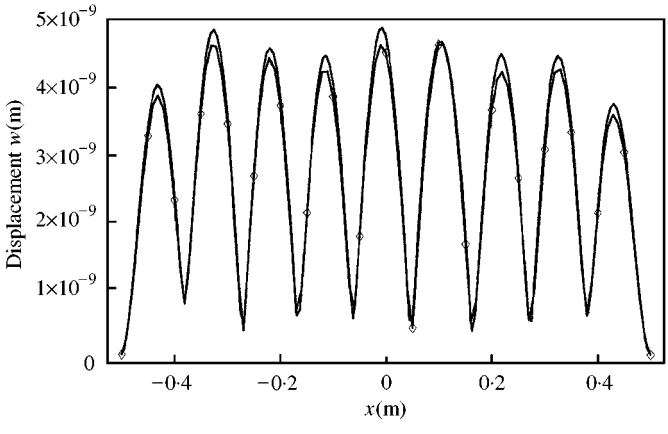

Figure 7. Comparison between methods I and II (marked with ◇) for plate 2 at 1500 Hz.

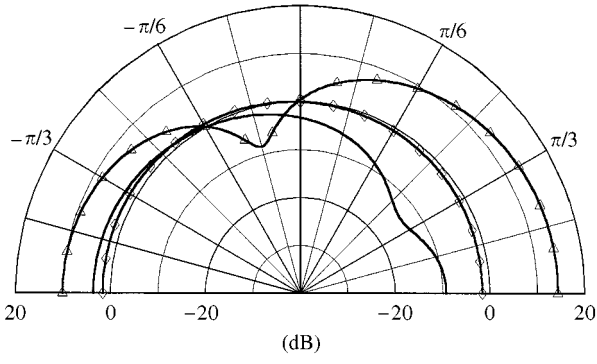

Figure 8. Directivity pattern at 1 m. Plate 1 (continuous line), plate 2 (marked with ◇) and plate 3 (marked with △) at 56 Hz.

It has been shown that for both methods, the convergence does not depend only on the wavelengths in the fluid and in the plate. The coupling factor is also an important parameter. The comparison of Tables 2 and 3 provides an interesting result. The rules of convergence are different with methods I and II. With method I, the effect of the coupling

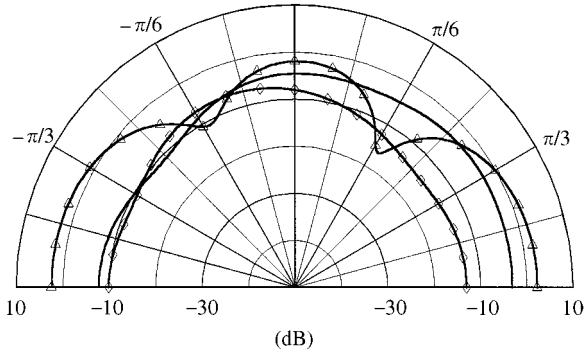

Figure 9. Directivity pattern at 1 m. Plate 1 (continuous line), plate 2 (marked with ◇) and plate 3 (marked with △) at 1500 Hz.

factor is clearly essential when the wavenumbers are equal (as for plates 1 and 2). With method II, the values of the wavenumber in the plate (or the number M of maxima) is the main parameter.

4. RESPONSE OF A THIN PLATE TO A TURBULENT WALL PRESSURE EXCITATION

The aim of this section is the prediction of the response of a simple structure—a two-dimensional baffled rectangular plate—induced by a turbulent flow, that is the determination of the various power density spectra (displacement and pressure fields). The calculation of these spectra is based on the solution of the fluid-loaded plate equation for a continuous set of harmonic excitations. The method used here is based on the expansion of the unknown functions in series of Tchebycheff polynomials and adapted collocation equations, as described in section 3.2.2.

The plate is made of purely elastic steel characterized by: Young's modulus $E = 2{\cdot}0 \times 10^{11}$ Pa, Poisson ratio $\nu = 0{\cdot}3$, density $\mu = 7800\ \mathrm{kg/m^3}$; its size is $1{\cdot}0 \times 0{\cdot}7\ \mathrm{m^2}$; with thickness $h = 0{\cdot}05$ m.

One of the two half-spaces is occupied by water, with density $1000\ \mathrm{kg/m^3}$ and sound velocity 1500 m/s. The other half-space is a *vacuum*.

The plate is excited by a turbulent flow parallel to its longest sides. There is no acoustic source. The acoustic fluid loading of the plate is modelled as if the fluid was at rest: indeed, a few numerical experiments have shown that, for small Mach numbers, the fluid velocity has a quite negligible influence on the acoustic pressure on the plate.

4.1. MODEL USED FOR THE TURBULENCE AND RESPONSE OF THE PLATE TO THE CORRESPONDING WALL PRESSURE

The turbulent wall pressure excitation, which is a space–time random process, is characterized by a cross-power density spectrum [19] $\Phi_p(x, y; x', y'; \omega)$ where ω is the angular frequency. Among the many models available in the literature (see for example references [20] or [21]), we have chosen the one proposed by Corcos who adopts the following form for the wall pressure:

$$\Phi_p(x, y; x', y'; \omega) = \Phi_p^0(\omega)\, \mathrm{e}^{-\alpha_x \omega |x - x'|/U_c}\, \mathrm{e}^{-\alpha_y \omega |y - y'|/U_c}\, \mathrm{e}^{\mathrm{i}\omega(y - y')/U_c} \tag{40}$$

with $\alpha_y = 0{\cdot}1$, $\alpha_x = 7\alpha_y$ and $U_c = 0{\cdot}7U_\infty$. Following reference [22], the spectrum $\Phi_p^0(\omega)$ is defined by

$$\log_{10} \Phi_e(\omega) = -5{\cdot}1 - 0{\cdot}9 \log_{10} f_e - 0{\cdot}34 (\log_{10} f_e)^2 - 0{\cdot}04(\log_{10} f_e)^3$$

$$\text{with} \quad f_e = \omega\delta/2\pi U_\infty \,, \quad q_0 = 1/2\mu_0 U_\infty^2 \,, \quad \Phi_p^0(\omega) = (q_0\delta/U_\infty)\Phi_e(\omega), \tag{41}$$

where $\delta = 0{\cdot}10$ m is the turbulent boundary layer thickness.

As shown in many papers (in particular in reference [8]), the cross-spectral density $S_u(M, M'; \omega)$ of the plate displacement is related to the cross-spectrum density of the excitation by

$$S_u(M, M'; \omega) = \int_\Sigma \int_\Sigma u(Q, M; \omega)\, \Phi_p(Q, Q'; \omega)\, u^*(Q', M'; \omega)\, \mathrm{d}Q\, \mathrm{d}Q', \tag{42}$$

where $u(Q, M; \omega)$ is the response of the fluid-loaded plate to a harmonic unit point force δ_Q and u^* is the complex conjugate of u. The numerical problem is the determination of the plate displacement u for a harmonic excitation.

4.2. MAIN STEPS OF THE COMPUTATION AND RESULTS

The computation of $u(M, Q; \omega)$ was made with the numerical method presented in section 3.2.2. The acoustic pressure on the plate surface is described by the Green representation corresponding to a fluid at rest. The Green representation of the plate displacement is used: it involves boundary layer integrals to account for the boundary conditions. The Green representation of the plate displacement, the continuity condition between the plate displacement and the normal component of the fluid particle displacement, and the boundary conditions provide a system of four integral equations.

The unknown functions which depend on one variable—the two layer densities—are expanded into truncated series of Tchebycheff polynomials. The unknown functions which depend on two variables—the plate displacement and the acoustic pressure on the plate surface—are expanded into truncated series of products of two Tchebycheff polynomials. The coefficients of these expansions are evaluated by an adapted collocation method. A detailed presentation of this specific case is given in reference [7].

The last step is the evaluation of the power density spectrum of the displacement. This requires the computation of quadruple integrals. But, due to the variable separation of both the plate displacement representation and the power density spectrum of the excitation, the calculation is reduced to the evaluation of the product of two double integrals.

Figure 10 presents an example of the response of the plate excited by a turbulent boundary layer. The power density spectrum of the plate velocity $S_v = \omega^2 S_u$ has been calculated for two different conditions. The continuous curve is the response of the water-loaded plate. It is compared to the response of the *in vacuo* plate excited by the same wall pressure. This clearly shows the fluid-loading influence. The two curves are obtained for $x = 0{\cdot}9L_x$ and $y = 0{\cdot}9L_y$. With this location, all the modes of the plate are visible. The fluid loading has two consequences which can be observed on these curves: the added mass effect, that shifts the peaks toward the low-frequency domain, and the damping effect, that reduces their amplitude. The positions of the amplitude maxima are compared to the resonance frequencies of the fluid-loaded plate (see Table 4). One can see that the maxima of the response of the plate occur for frequencies which are very close to the real part of the

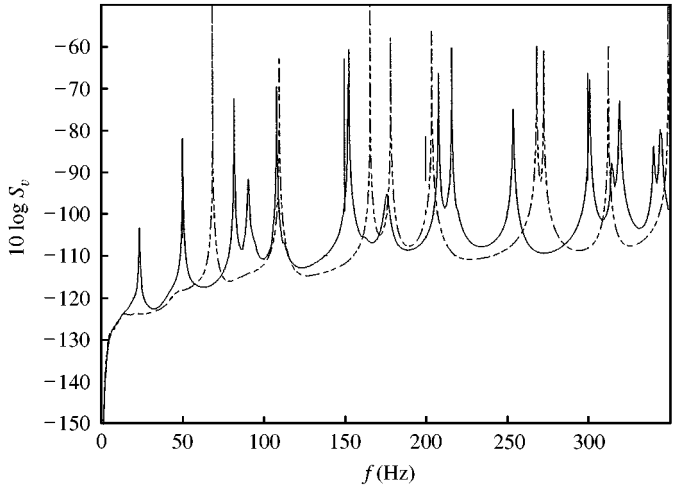

Figure 10. Power spectral density of the velocity of the plate at $x = 0{\cdot}9L_x$, $y = 0{\cdot}9L_y$: ——, power spectral density of the velocity in water; – – – – –, power spectral density of the *in vacuo* velocity.

TABLE 4

Resonance frequencies of the plate and peak frequencies of the plate velocity power density spectrum

Mode no.	Resonance frequencies (Hz)	Peak frequencies of S_v (Hz)
1	$23{\cdot}5\ (1 - i8{\cdot}1 \times 10^{-3})$	23·6
2	$50{\cdot}2\ (1 - i2{\cdot}0 \times 10^{-5})$	50·3
3	$81{\cdot}9\ (1 - i6{\cdot}1 \times 10^{-5})$	81·9
4	$90{\cdot}7\ (1 - i4{\cdot}4 \times 10^{-3})$	90·6
5	$108{\cdot}2\ (1 - i4{\cdot}6 \times 10^{-5})$	108·3
6	$152{\cdot}3\ (1 - i2{\cdot}6 \times 10^{-4})$	152·3
7	$152{\cdot}5\ (1 - i5{\cdot}2 \times 10^{-5})$	152·9
8	$173{\cdot}9\ (1 - i7{\cdot}5 \times 10^{-3})$	176·0
9	$205{\cdot}3\ (1 - i2{\cdot}4 \times 10^{-4})$	208·2
10	$216{\cdot}4\ (1 - i1{\cdot}4 \times 10^{-5})$	216·4
11	$252{\cdot}7\ (1 - i1{\cdot}0 \times 10^{-3})$	254·2
12	$301{\cdot}2\ (1 - i3{\cdot}6 \times 10^{-4})$	301·4
13	$314{\cdot}1\ (1 - i1{\cdot}0 \times 10^{-3})$	315·0
14	$320{\cdot}2\ (1 - i3{\cdot}7 \times 10^{-4})$	320·0
15	$340{\cdot}4\ (1 - i1{\cdot}1 \times 10^{-3})$	341·0
16	$346{\cdot}3\ (1 - i4{\cdot}3 \times 10^{-5})$	345·0

resonance frequencies; their amplitudes get smaller as the damping of the resonance modes increases. For example, the response of the plate close to 82 and 90 Hz presents a difference of more than 20 dB. This could be expected simply by looking at the resonance frequencies: at 90 Hz the resonance frequency has an imaginary part 100 times greater than the one at 82 Hz. The mode that corresponds to 90 Hz is significantly damped by the fluid loading. One can also remark that the resonance modes which present a high damping are modes with a maximum amplitude at the center of the plate (this occurs for the first, fourth, eighth, etc., modes).

This example clearly shows that, for an excitation with a wide frequency band, the response of the system structure/fluid is governed by the fluid-loaded modes. It also suggests that a refined mesh is required around each resonance frequency, while a rather large frequency mesh or an interpolation algorithm between two successive resonance frequencies is sufficient. In our opinion, the use of the resonance modes representation of the structure response is certainly one of the best methods, if not the best. The example of the next section seems to confirm the assertion.

5. DIFFRACTION OF A TRANSIENT ACOUSTIC WAVE BY A *LINE*-2′ SHELL

The shell *Line*-2′ is composed of three elementary thin shells Σ_1, Σ_2 and Σ_3. The elements Σ_1 and Σ_3 are two identical hemi-spherical end-caps which close the extremities of a cylindrical element Σ_2. They all have the same mean radius R and the same thickness h which is assumed to be a few percents of R; the length of the cylindrical part is $2L$.

The three elements are made of the same material, characterized by a density ϱ_s, a Young modulus E and the Poisson ratio ν.

A co-ordinate system is associated with each element (see Figure 11). The shell is immersed in a fluid, water, extending to infinity and is excited by an incident transient wave.

As described in section 2.2, the response of the system is sought as a series of the fluid-loaded resonance modes of the shell and of the corresponding radiated acoustic pressure. The resonance modes are computed with the method described in section 3.3. The details concerning this example are presented in references [12, 15].

5.1. MAIN STEPS OF THE NUMERICAL PROCEDURE

The first step is to compute the resonance modes. This requires one to solve the homogeneous equations governing the harmonic regime.

Because the structure has an axis of symmetry, it is possible to expand all the unknown quantities—the shell displacement (three components), the layer density and the corresponding diffracted acoustic pressure—into Fourier series of the angular variable φ.

The angular harmonics of the shell displacement components and of the layer density satisfy a system of integro-differential equations of one variable only, the curvilinear abscissa along a meridian of the shell. Because of the spherical end-caps, variable coefficients occur. The shell displacement is approximated by polynomial functions (linear combinations of Legendre polynomials) which satisfy the boundary conditions at the poles and the continuity conditions at the junctions of the spherical parts of the shell and the cylindrical part. The layer density is approximated by a truncated series of Legendre polynomials. Use is made of Ritz–Galerkin equations for the shell equation and of adapted collocation equations for the continuity relationship between the normal component of the shell displacement and of the fluid particle displacement.

A very straightforward method is used to calculate the transient response of the shell. For each angular harmonic, each component of the shell displacement is expressed as a linear combination of the corresponding component of the modal resonance displacements; the layer density is expressed as a linear combination of the modal resonance layer densities. These four expansions, which are considered as independent, are introduced into the variational form of the governing time-dependent equations. Using the modal resonance displacement components and the modal resonance layer densities as test functions, one obtains a system of linear algebraic equations which provides the unknown coefficients.

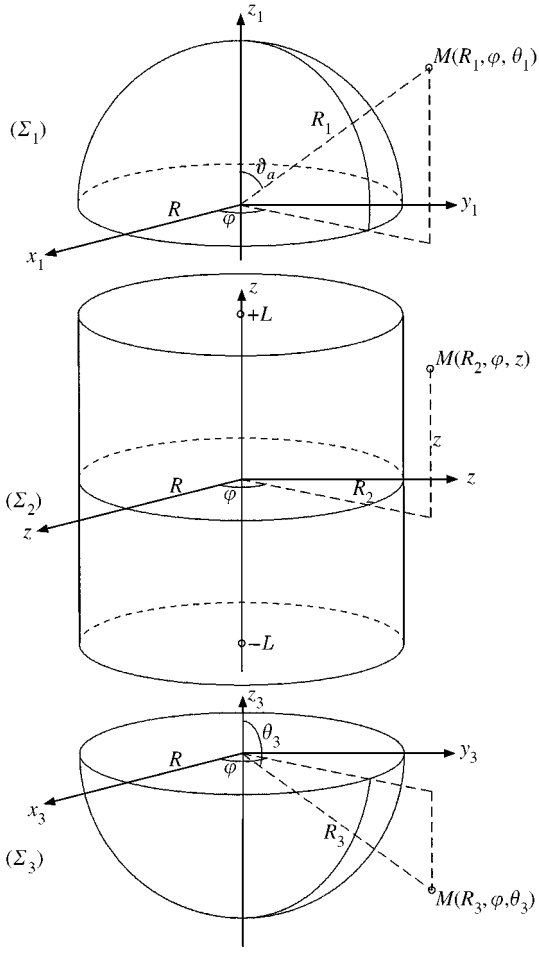

Figure 11. Geometry of *Line*-2′ and the three co-ordinate systems.

5.2. COMPARISON BETWEEN NUMERICAL PREDICTIONS AND EXPERIMENTAL RESULTS

A *Line*-2′ shell, made of an aluminum alloy, has been used for experiments. Its radius is 0·020 m, its total length is 0·080 m and its thickness is 0·001 m. Its mechanical characteristics are: density = 2611 kg/m^3, Young's modulus $0{\cdot}81 \times 10^{11}$ Pa, the Poisson ratio = 0·30. It was immersed in a large water tank with anechoic boundaries. An acoustic transducer, located on the symmetry axis of the target, was used for the generation of a short signal with a spectrum centered around 250 kHz (four oscillations, lasting 0·2 ms). A unique transducer was used for the sound emission and the recording of the reflected wave. The reflected wave in the backward direction was recorded 1 m away from the shell.

In Figure 12, the experimental signal is compared with the predicted one, for a total time interval of 2·0 ms, that is 10 times the duration of the incident wave. It must be noticed that the reflected wave is very sensitive to the relative positions of the transducer and of the target: a small error in the orientation of the target can change the diffracted wave by a rather large amount. Nevertheless, the agreement between the two curves is very good.

Though the reflected signal was computed as a whole, the specular reflection and the successive wave packets, which correspond roughly to creeping waves having travelled

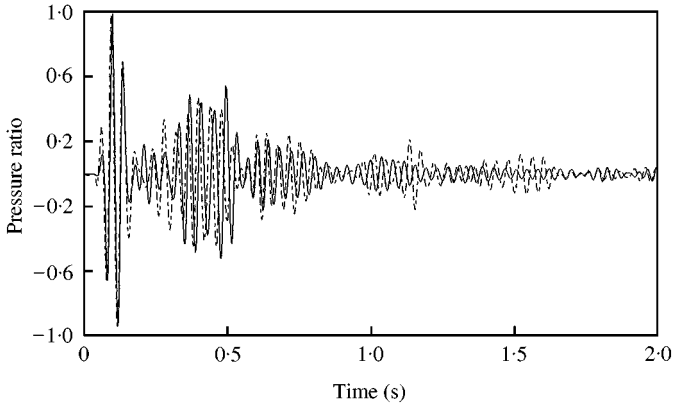

Figure 12. Comparison between measurement and prediction of the time-dependent sound field diffracted in the axial incidence direction by a *Line*-2′ shell made of aluminum alloy with radius $R = 0{\cdot}02$ m, total length $4R$ and thickness $h = 0{\cdot}001$ m: ——, computed signal; – – – – –, measured signal.

several times around the target, appear clearly. This shows the strong efficiency of the expansion of the diffracted acoustic transient pressure in terms of the resonance modes.

6. CONCLUSION

The aim of this paper was to point out the efficiency of the resonance modes of the fluid-loaded structure to describe the response of a coupled system structure/fluid to any excitation and more specifically to a transient excitation.

In all the examples presented, the fluid is water, because, in a heavy fluid, the resonance modes are far from the *in vacuo* modes and cannot be easily deduced from them, as, for example, by a perturbation method.

The resonance modes are obtained by solving the equations corresponding to a harmonic regime with a complex frequency. Several numerical methods have been tested, to determine some practical rules of convergence. The effect of the heavy fluid is pointed out. It is shown that these rules depend on two main parameters: the wavenumber in the plate and the coupling factor.

Then two examples are presented. The first one corresponds to a baffled plated excited by a turbulent wall pressure. A numerical comparison shows the influence of the fluid on the response of the system and the importance of the resonance modes which, obviously, govern the power density spectrum of the system response.

The second example corresponds to a thin shell excited by a transient acoustic wave. The signal diffracted by the shell is expressed as a series of resonance modes and is compared with experimental results obtained in a water tank. The quality of the agreement between numerical predictions and experiments points out that the resonance modes series is certainly one of the best tools to solve this class of problems.

The authors have been very pleased with the opportunity which has been offered them to write a paper for the birthday of their friend Philip Doak. They are sure that, as usual, Phil will have comments and criticisms .... They suggest that this discussion takes place when he likes at *Les Arcenaux*, where fish and wine are still gorgeous!

REFERENCES

1. M. C. JUNGER and D. FEIT 1993 *Sound, Structures, and Their interaction*. Acoustical Society of America (1972 and 1986 by Massachusetts Institute of Technology).
2. F. FAHY 1985 *Sound and Structural Vibration*. London: Academic Press.
3. C. LESUEUR 1988 *Rayonnement acoustique des structures*. Collection de la Direction des Etudes et Recherches d'Electricité de France, Eyrolles, Paris.
4. R. OHAYON and C. SOIZE 1998 *Structural Acoustics and Vibration*. London: Academic Press.
5. D. HABAULT 1999 *Fluid-structure Interactions in Acoustics*. CISM Courses and Lectures N. 396. Wien—New York: Springer.
6. D. G. CRIGHTON 1989 *Journal of Sound and Vibration* **133**, 1–27. The 1988 Rayleigh medal lecture: fluid loading—the interaction between sound and vibration.
7. P.-O. MATTEI 1996 *Journal of Sound and Vibration* **196**, 299–315. A two-dimensional Tchebycheff collocation method for the study of the vibration of fluid-loaded rectangular plate.
8. P. J. T. FILIPPI and D. MAZZONI 1997 In *Uncertainty Modeling in Finite Element, Fatigue and Stability of Structures*, (Prof. Ayyub, Prof. Guran and Prof. Haldar, editors), Vol. 9 of *Series on Stability, Vibrations and Control of Systems*, 117–158. Singapore: World Scientific Publisher. Chapter 5. Response of a vibrating structure to a turbulent wall pressure: fluid-loaded structure modes series and boundary element method.
9. D. HABAULT and P. J. T. FILIPPI 1998 *Journal of Sound and Vibration* **213**, 333–374. Light fluid approximation for sound radiation and diffraction by thin elastic plates.
10. S. MARTIN-SEIGLE, M.-C. PÉLISSIER and P. J. T. FLIPPI 1999 *Flow, Turbulence and Combustion* **61**, 71–83. Euromech 369 special issue. Acoustic radiation from a finite length cylindrical shell excited by an internal acoustic source: solution based on a Boundary Element Method and a matched asymptotic expansion.
11. C. DURANT, G. ROBERT, P. J. T. FILIPPI and P.-O. MATTEI 2000 *Journal of Sound and Vibration* **229**, 1115–1155. Vibroacoustics response of a thin cylindrical shell excited by a turbulent internal flow: comparison between numerical prediction and experimentation.
12. C. MAURY and P. J. T. FILIPPI *Journal of Sound and Vibration* (accepted for publication). Transient acoustic diffraction and radiation by an axisymmetrical elastic shell: a new statement of the basic equations and a numerical method based on polynomial approximations.
13. G. M. CORCOS 1963 *Journal of the Acoustical Society of America* **35**, 192–199. Resolution of pressure in turbulence.
14. P. M. MORSE and K. U. INGARD 1968 *Theoretical Acoustics*. New York: McGraw Hill.
15. C. MAURY 1999 Thèse de mécanique—spécialité: Acoustique et dynamique des vibrations, Université de la Méditerranée. *Rayonnement acoustique de structures vibrantes: études en régimes temporels et fréquentiels*.
16. C. BARDOS, M. CONCORDEL and G. LEBEAU 1989 *Journal d'Acoustique* **2**, 31–38. Extension de la théorie de la diffusion pour un corps élastique immergé dans un fluide. Comportement asymptotique des résonances.
17. R. KRESS 1989 *Linear Integral Equations*. Series in Applied Mathematical Sciences 82. New York: Springer-Verlag.
18. P. JUHL 1998 *Journal of Sound and Vibration* **212**, 703–719. A note on the convergence of the direct collocation boundary element method.
19. D. G. CRIGHTON, A. P. DOWLING, J. E. FFOWCS WILLIAMS, M. HECKL and F. G. LEPPINGTON 1992 *Modern Methods in Analytical Acoustics*. Lecture Notes. London: Springer-Verlag.
20. W. R. GRAHAM 1997 *Journal of Sound and Vibration* **206**, 541–565. A comparison of models for the wavenumber-frequency spectrum of turbulent boundary layer pressures.
21. W. K. BLAKE 1986 *Mechanics of Flow-Induced Sound and Vibration. Vols.* 1 *and* 2. London: Academic Press.
22. C. DURANT 1999 Ph.D. thesis. École Centrale de Lyon, LMFA, UMR 5509. *Etude expérimentale de l'excitation et de la réponse vibro-acoustique d'une conduite sollicitée par un écoulement interne*.